

The influence of filtering the power spectrum and adding thermal energy on
the structure of dark matter halos

Vladimir Avila-Reese and Pedro Colín

Instituto de Astronomía, U N A M., A P. 70-264, 04510, México, D F., México

Octavio Valenzuela

Astronomy Department, New Mexico State University, Box 30001, Department 4500, Las Cruces,
NM 88003-0001, USA

Elena D'Onghia

Università degli Studi di Milano, via Celoria 16, 20100 Milano, Italy

and

Claudio Firmani

Instituto de Astronomía, U N A M., A P. 70-264, 04510, México, D F., México

A B S T R A C T

We explore the density profiles of dark matter halos formed in high-resolution cosmological N -body simulations with power spectra of density fluctuations damped below a given length scale R_f . The density profile shape of halos with masses smaller than the mass M_f corresponding to R_f does not significantly differ from that of the cold dark matter (CDM) halos; on the average, this shape is well described by the Navarro, Frenk, & White profile. However, the concentration of halos less massive than M_f remains constant as the mass decreases, while for the CDM halos the concentration increases. The cosmology of the former halos is not hierarchical but due to fragmentation of pancakes, their typical formation epoch being slightly later than that of halos of mass close to M_f . The lower concentrations of these halos relative to the CDM ones may be explained by their late formation.

If the suppression of power is associated with the free-streaming damping characteristic for warm dark matter (WDM) particles, then particles will have a residual thermal velocity dispersion v_{th} . We have included this velocity dispersion in our simulations and have found that its influence on the halo structure is negligible. Using an analytical formalism, we show that halos formed by monolithic collapse will present a significant soft core only when particles have velocity dispersions much larger than the v_{th} of warm particles. Relative to CDM, in a WDM model with $R_f = 0.15 - 0.20$ Mpc (at cosmology with $\Omega_m = h = 0.7$) we find that not only the number of satellite galaxies in Milky-Way systems is in better agreement with the observations, but also the concentrations, the Tully-Fisher relation, and the formation epochs of dwarf galaxies.

1. Introduction

The damping of moderate high-frequency modes in the power spectrum of density fluctuations has been proposed to overcome potential observational difficulties at small scales of the hierarchical cold dark matter (CDM) scenario for structure formation (e.g., Avila-Reese, Firmani, & Hernandez 1998; Moore et al. 1999b; Sommer-Larsen & Dolgov 2000; Hogan 1999; Kamionkowski & Liddle 1999; Hogan & Dalcanton 2000; White & Croft 2000; Colín, Avila-Reese, & Valenzuela 2000). The damping of small-scale modes in the power spectrum may be produced either during its primordial generation (in the biased scalar inflationary models, for example) or due to Landau and free-streaming damping, which erase galactic or subgalactic density fluctuations when the dark matter particles are warm (e.g., Blumenthal, Pagels, & Primack 1982); although the free-streaming damping could also be present in CDM models if CDM particles are non-thermally produced (Lin et al. 2000). In this paper we study warm dark matter (WDM) models, however, it is important to remark that our results are also valid for other models where the power spectrum is suppressed.

A possible shortcoming of the CDM scenario is the large excess of substructure in Milky Way-like halos; upon the understanding that in each small halo a dwarf galaxy forms, the number of satellites predicted by this cosmology is by far more than the number of observed satellites around the Milky Way and Andromeda galaxies (Kauffmann et al. 1993; Klypin et al. 1999; Moore et al. 1999a; but see van Kampen 2000 for a criticism on numerical results). The cosmological N -body experiments of Colín et al. (2000; hereafter Paper I) have shown that the observed satellite circular velocity function of the Milky Way and Andromeda can be reproduced if the power spectrum is exponentially damped (filtered) at scales $0.1 - 0.2$ Mpc (a flat cosmological model with $\Omega = 0.7$ and $h = 0.7$ was used). A free-streaming scale R_f of $0.1 - 0.2$ Mpc is attained for a particle mass m_W of $0.6 - 1$ keV (Sommer-Larsen & Dolgov 2000). Interestingly, Narayanan et al. (2000) derived a lower limit for m_W of 750 eV from the restriction that the predicted power spectrum should reproduce the observed properties of the Lyman forest in quasar spectra.

In Paper I we also found that the concentrations of the guest WDM halos decrease as R_f increases (i.e., as m_W decreases), being these concentrations smaller than those corresponding to the guest CDM halos. The density profiles of most of these halos do not dramatically deviate from the Navarro, Frank, & White (NFW, 1997) profile but it should be emphasized that the density profiles were not determined with accuracy because guest halos were only resolved with a small number of particles. A second potential problem of the CDM scenario is related namely to the inner density profile and/or concentration of small halos: there is an apparent discrepancy between numerical simulation results and observations (e.g., Moore 1994; Flores & Primack 1994; Burkert 1995; de Blok & McGaugh 1997), although more recent observational studies have challenged this conclusion (van den Bosch et al. 2000; Swaters, Madore & Trewheella 2000; van den Bosch & Swaters 2000).

In the present paper we study in more detail the density profiles of WDM halos with masses close to or smaller than the free-streaming mass, M_f , in order to explore whether they offer a better

to observations. It is important to notice that the cosmogony of these halos is not hierarchical. Halos with masses near or larger than M_f by factors of to 5–10 assemble a large fraction of their present-day mass relatively late (monolithic collapse), whereas halos with masses smaller than M_f form from the gravitational fragmentation of larger pancake-like structures, as in the "top-down" scenario (Zeldovich 1970). Firmani et al. (2000b) emphasized that the density profiles of dark halos formed through a monolithic collapse depend significantly on the 3-D velocity dispersion of the collapsing particles (see also Aguilar & Merrit 1990); this velocity dispersion may be primordial (thermal relic) or can be acquired during an inhomogeneous gravitational collapse.

The non-zero thermal velocities of warm particles (warm ions) should produce shallow halo cores because of the phase packing or Liouville limit (e.g., Hogan & Dalcanton 2000). However, this thermal velocity dispersion v_{th} for warm ions with masses of ~ 1 keV seems to be too small to produce significant cores. In Paper I this velocity was neglected, remaining uncertain the effect it could have on the structure of simulated halos (Sellwood 2000). Here we will introduce v_{th} and explore whether a shallow core forms in virialized halos. An analytical approach will be also used to study the "hot" monolithic collapse.

After the completion of this paper, a similar paper by Bode, Ostriker, & Turok (2000) appeared in the preprint list of Los Alamos National Laboratory. The results presented by Bode et al. nicely complement those given here. Besides, Bode et al. suggest a series of observational tests to verify the predictions of WDM models.

In §2 we discuss the WDM models explored in this paper. In §3 we describe briefly the numerical simulations. In §4 we present results from our experiments aiming to explore the density profiles and concentrations of halos with masses below the mass corresponding to the filtering scale. The influence of a non-zero thermal velocity of warm ions on the halo structure is studied in §4.1. Section 5 is devoted to analytical and numerical studies of the hot monolithic collapse. In §6.1 we describe and discuss how structure formation proceeds in simulations with a power spectrum suppressed at small scales. The viability of the WDM scenario is discussed in §6.2. Finally, our conclusions are given in §7.

2. Cosmological Models

As in Paper I here we also use flat Λ CDM and WDM cosmological models with $\Omega_m = 0.7$, $h = 0.7$, and $\Omega_b = 1$. These models can account successfully for many observational facts from the cluster mass estimates (e.g., Carlberg et al. 1996) to the distribution of galaxies (e.g., Peacock & Dodds 1994) and the evolution of the cluster abundance (e.g., Eke et al. 1998). More recently, the observations of the microwave background anisotropy at small scales ($36 \leq l \leq 785$) by BOOMERANG (de Bernardis et al. 2000) and MAXIMA (Balbi et al. 2000) point to a value for the total density of the Universe Ω_{tot} (in units of the energy density for closure) close to 1 ($\Omega_{tot} = \Omega_m + \dots$). By combining this result with measurements of high-redshift supernovae (Perlmutter et al. 1999;

Riess 1998; Schmidt et al. 1998) the resulting contribution from a cosmological constant to the density of the universe is 0.5–0.8 results.

Two characteristics distinguish WDM from CDM. The damping of the small-scale density fluctuations and the fact that thermal velocity dispersion might not be negligible at the time of structure formation. The free-streaming length R_f is related to the mass of the warm ion through the following equation (e.g., Sommer-Larsen & Dolgov 2000):

$$R_f = 0.2 \left(\omega_{\text{WDM}} h^2 \right)^{1/3} \frac{m_{\text{W}}}{1 \text{keV}}^{4/3} \text{ Mpc}; \quad (1)$$

where ω_{WDM} is the contribution to the energy density of the universe from WDM¹. We follow Sommer-Larsen & Dolgov and define a characteristic free-streaming wavenumber k_f as the k for which the WDM transfer function is one half; that is, $k_f = 0.46/R_f$. The definition of a characteristic filtering mass M_f given a filtering length has not been uniquely defined and thus has introduced some confusion in the literature; its value can vary by about three orders of magnitude from one definition to another. For instance, if we define M_f simply as $4/3 R_f^3$ and compare it with the definition by Sommer-Larsen & Dolgov, we then find that the M_f value given by the latter definition is a factor of 318 greater than the M_f value obtained by the former one. We follow Sommer-Larsen & Dolgov to define the filtering mass:

$$M_f = \frac{4}{3} \omega_{\text{WDM}} \frac{m_{\text{W}}^3}{2}; \quad (2)$$

where $k_f^2 = 2/k_s = 13.6/R_f$. This definition of M_f is justified by the numerical experiments of Tittley & Couchman (1999). They found that the initial density distribution produced by a sharp cut in the power spectrum at $k_c = 2/k_s$ (the exponential drop in the power spectrum in our case is at $k_c = 2/k_f$) is similar to that one produced when the initial density field is convolved with a top-hat window of smooth radius $k_s = 2$. The analysis of the halo properties below show that the mass at which the WDM halos begin to diverge from the CDM ones is just around the mass given by eq. (2).

The WDM power spectrum we use is that given by Bardeen et al. 1986:

$$P(k) = T_{\text{WDM}}^2(k) P_{\text{CDM}}(k); \quad (3)$$

where the WDM transfer function is approximated by

$$T_{\text{WDM}}(k) = \exp \left[-\frac{k R_f}{2} - \frac{(k R_f)^2}{2} \right]; \quad (4)$$

and P_{CDM} is the CDM power spectrum given by Klypin & Holtzman (1997) (see Paper I).

¹Modifications to eq. (1) exist; for example, a larger coefficient of proportionality is given by Pierpaoli et al. 1997. Using their coefficient, for a given R_f , m_{W} should be roughly two times larger than the values used here.

3. The Numerical Simulations

The simulations were performed using the multiple-mass scheme variant of the Adaptive Refinement Tree (ART) N-body code (Kavtsov, Klypin, & Khokhlov 1997). The ART code achieves high spatial resolution by refining the base uniform grid in all high-density regions with an automated refinement algorithm. The multiple-mass scheme is used to increase the mass and spatial resolution in few selected halos and its implementation is described in detail elsewhere (Klypin et al. (2000); see also Paper I). The major changes are made in the initial conditions.

We start our simulations by making a low-resolution run with 32^3 or 64^3 particles in which all particles have the same largest possible mass. We use these runs to select potential host halos to be re-simulated with higher mass and force resolution. We then identify all particles within ≈ 2 virial radii and trace back them to get their Lagrangian positions at $z = 40$. Next the initial distribution with the different particle masses is generated and the models are evolved with the multiple-mass variant of ART. Models with $R_f = 0.2$ Mpc have four mass levels (particles with masses 1, 8, 64, $256 m_p$) whereas models with $R_f = 1.7$ Mpc have three. The mass resolution on the finest mass level corresponds to a box of 256^3 particles in both series of simulations.

As in Paper I the Bound Density Maxima (BDM) grouping algorithm was used to locate the host halos in the low mass resolution. The BDM algorithm finds the positions of local maxima in the density field smoothed at the scale of interest and applies physically motivated criteria to test whether a group of particles is a gravitationally bound halo. The BDM is also used to find the host and guest halos in the multiple-mass high resolution simulations.

In Table 1 we present an overview of all the simulations used in this paper. The first two simulations have $R_f = 0.2$ Mpc ($m_W = 605$ eV) and are used to explore the effect of the non-zero thermal velocity of warm ions on the internal structure of simulated halos. In simulation WDM we include explicitly the thermal velocity component v_{th} in the initial conditions, while in simulation WDM $v_{th} = 0$. The host halo has little less than a million of particles while guest halos are resolved with thousands of particles. The formal force resolution (column 6) is measured by the size of a cell in the finest refinement grid, and the mass per particle (column 4) is the mass for those particles that belong to the finest level of mass resolution.

The next series of simulations, WDM_{7.5}, WDM₁₅, WDM₃₀, and WDM₆₀, in which we set $R_f = 1.7$ Mpc (which corresponds to $M_f = 1.7 \cdot 10^{14} h^{-1} M_\odot$) but vary the size of the box, were aimed at studying the density profiles and concentrations of halos with virial masses close to or below the corresponding filtering mass. The virial masses of host halos in these simulations are more and more away from M_f as the box size is reduced. These halos are resolved with a number of particles which goes from $4 \cdot 7 \cdot 10^4$ particles (model WDM₆₀) to $3 \cdot 10^5$ particles (models WDM_{7.5} and WDM₁₅). For comparison, we also run a CDM simulation ($R_f = 0$) with the same initial conditions of the WDM₆₀ simulation (CDM₆₀).

One could think that by reducing the box size, a higher mass resolution is achieved as it

happens in CDM simulations. This does not happen however for models with damped power spectrum because the characteristic host halo mass in the box becomes smaller as the box size decreases. The box needs, moreover, to be sufficiently big in order for the fundamental mode ($k_0 = 2\pi/L_{\text{box}}$) to be much smaller than k_f and thus to sample fairly the high-frequency region of the power spectrum. For $R_f = 1.7 \text{ Mpc}$, for example, the filtering wave number is $0.38 h \text{ Mpc}^{-1}$ which means that the size of the box L_{box} has to be larger than $16 h^{-1} \text{ Mpc}$. By reducing L_{box} below $16 h^{-1} \text{ Mpc}$ we will not get a higher mass resolution because large halos (with more particles) will not form. On the other hand, the omission of wavelengths larger than $16 h^{-1} \text{ Mpc}$ will probably affect the structure of the halos.

In order to attain a visual impression of how a WDM halo looks, in Fig. 1 we present the distribution of particles of a host halo from model WDM₆₀ at $z = 0$ and $z = 1.0$. In the bottom panel, all particles within a sphere of radius $1.5 h^{-1} \text{ Mpc}$ centered on the halo are plotted (the virial radius of this halo is $0.85 h^{-1} \text{ Mpc}$). We have traced back all particles shown in the bottom panel to $z = 1$ and plotted them in the top panel. All of them are within a sphere of radius $5.6 h^{-1} \text{ Mpc}$ comoving centered on the center of mass of the particle system.

4. The structure of halos with masses near or below the filtering mass

In Paper I host halos of a few $10^{12} h^{-1} \text{ M}_\odot$ were re-simulated within the multiple-mass scheme in a box size of $15 h^{-1} \text{ Mpc}$. The formal force resolution was of $0.45 h^{-1} \text{ kpc}$ and the mass per particle in the next level of resolution corresponded to $1.66 \cdot 10^7 h^{-1} \text{ M}_\odot$. Thus, the guest halos reported in Paper I (those with scales below the filtering scale) were poorly resolved, they only have few $10^2 - 10^3$ particles, a number not high enough to study in detail their density profiles. We can reduce the box size in order to improve the mass resolution but not by much because it soon shows the effect mentioned in section 3.

Since in the present paper we are concentrated on exploring the density profiles of those halos with scales near or below R_f , it was not relevant which R_f we chose. An $R_f = 1.7 \text{ Mpc}$ was chosen which corresponds to a filtering mass of $M_f = 1.7 \cdot 10^{14} h^{-1} \text{ M}_\odot$ (see x2). For model WDM₆₀ four host halos were re-simulated. These halos have $4 - 7 \cdot 10^4$ particles and their masses M_h range from 4 to $8 \cdot 10^{13} h^{-1} \text{ M}_\odot$,² i.e. they are $2 - 4$ times less massive than the corresponding filtering mass.

In Fig. 2 we show the density profiles obtained from simulations WDM₆₀ (filled circles) and CDM₆₀ (empty circles). The dashed lines are the NFW fit to the WDM halo. One clearly

²The halo mass M_h is the mass contained within the radius r_h , defined as the minimum between the virial radius r_{vir} and the truncation radius (where the spherically averaged outer density profile attains or increases). The virial radius is defined as the radius at which the average halo density is 334 times the background density. Almost all of the host halos attain the virial radius.

sees that the WDM halos are less concentrated than the CDM ones. Although both simulations started with identical initial conditions, the CDM halos resulted slightly more massive than the corresponding WDM ones (by factors $\sim 1.1 - 1.4$). The density profiles of the WDM halos follow roughly the NFW shape, but their fits are less good than those of the CDM halos. This is probably due to the late formation epoch of the former. In Figure 2 the inner density profiles are plotted up to four times the formal force resolution of the simulations (see Table 1). Only up to these radii the results are accurate. The WDM halos tend to have a shallower inner density profile.

In order to explore the structure of halos with masses much smaller than the filtering mass M_f we have run simulations with the same R_f but with box sizes of 30, 15 and 7.5 $h^{-1}Mpc$ (WDM_{30} , WDM_{15} , and $WDM_{7.5}$, respectively); in these simulations we find host halos with masses of $6 - 95 \cdot 10^{11} h^{-1}M$. As model $WDM_{7.5}$ has a very small box size, it only samples the high-frequency drop of the power spectrum; we thus expect the inner structure of the formed halo to be significantly affected.

In Fig. 3 we plot the density profiles of the four host halos obtained in the WDM_{30} model (continuous lines). Their masses range from 6.3 to $9.4 \cdot 10^{12} h^{-1}M$ containing from 4.7 to $7.1 \cdot 10^4$ particles, respectively. The long-dashed and dot-dashed lines are the density profiles for the only host halo obtained in the 15 $h^{-1}Mpc$ simulation ($M_h = 4.5 \cdot 10^{12} h^{-1}M$, about $3.54 \cdot 10^5$ particles) and in the 7.5 $h^{-1}Mpc$ simulation ($M_h = 5.7 \cdot 10^{11} h^{-1}M$, about $2.73 \cdot 10^5$ particles), respectively. For comparison, the density profile of a CDM halo of $2.5 \cdot 10^{12} h^{-1}M$ presented in Paper I is also shown (thick dashed line). We see that the difference in the concentrations of the density profiles of WDM and CDM halos are now even more significant than in the case of larger halos (Fig. 2). Nevertheless, the density profiles of these WDM halos, whose masses are much smaller than the filtering mass, can still be described by the NFW profile. The exception, as one expects (see x3), is the host halo from simulation $WDM_{7.5}$ which shows a prominent shallow core and a disturbed outer density profile.

The results obtained here confirm our previous claim: the WDM halos with masses near or below the filtering mass are less concentrated than the corresponding CDM halos (Paper I). In Figure 4 we plot the concentration versus halo mass M_h for the host halos obtained in the different models with $R_f = 1.7 Mpc$. We also include in this plot guest halos with more than 1000 particles (they are only a few). In panel (a) the concentration $c_{1=5}$ is defined as the ratio between the halo radius r_h and the radius where 1/5 of the total halo mass is contained (Avila-Reese et al. 1999). This definition of the concentration parameter is independent of the particular fitting applied to the halo density profile. The guest and host halos obtained in Paper I for a WDM model with $R_f = 0.2 Mpc$ are also shown in Fig. 4 (a) (crosses).

In order to compare the concentrations of WDM and CDM halos, we also plot in Fig. 4 (a) the results from our CDM simulation of box size 60 $h^{-1}Mpc$ as well as a linear fitting for thousands of isolated and clustered halos found in a CDM simulation (Avila-Reese et al. 1999). The trend in Fig. 4 (a) is clear: as the halo mass becomes smaller than the filtering mass, the $c_{1=5}$ concentration

departs more and more from the corresponding CDM $c_{1=5}$ concentration. Although the dispersion in the concentrations is big (see Fig. 8 in Avila-Reese et al. 1999 and Fig. 6 below) we feel that the trend seen in Fig. 4(a) for the WDM halos is real and is out of the statistical dispersion of the $c_{1=5} M_h$ relation of the CDM halos. For completeness, the concentrations obtained when fitting the density profiles of the halos from the $R_f = 1:7$ Mpc models to a NFW profile (\mathcal{G}_{NFW}) are presented in panel (b) of Fig. 4. The four halos obtained in the $60 h^{-1} \text{Mpc}$ CDM simulation as well as a linear interpolation for the $M_h c_{\text{NFW}}$ relation obtained from the CDM simulation presented in Avila-Reese et al. (1999), for halos whose density profiles are well described by the NFW shape, are also included in this plot.

4.1. Influence of the particle thermal velocity on the halo structure

As mentioned in the introduction, warm ons have a non-zero relict thermal velocity dispersion v_{th} , though for particle masses of $\sim 1 \text{ keV}$ this velocity dispersion is small (at $z = 40$, $v_{\text{th}} \sim 3 \text{ km/s}$ which is about 7 times smaller than the typical peculiar velocities at that epoch). A larger thermal velocity dispersion could be possible if warm ons self-interact; in this case the same free-streaming scale R_f can be attained with a smaller particle mass (Hogan 1999; Hannestad & Scherrer 2000) and, since $v_{\text{th}} / m_w \propto m_w^{-4/3}$, a smaller m_w implies a larger v_{th} . According to Hannestad & Scherrer (2000), the masses of the warm ons that produce a given free-streaming scale in the case of collisionless WDM might be 0.53 times smaller if warm ons self-interact. Therefore, the thermal velocity dispersion could be up to 2.3 times larger in the latter case.

We performed a simulation for a WDM model with $R_f = 0.2 \text{ Mpc}$ ($m_w = 605 \text{ eV}$) with the aim to explore the effect of a non-zero thermal velocity dispersion on the halo density profiles. The thermal velocities were randomly oriented and their magnitudes were drawn from a Fermi-Dirac phase space distribution with a rms velocity v_{th} twice higher than the one corresponding to this R_f value, making echo of the paper by Hannestad & Scherrer cited above. These velocities were added to the initial velocities computed using the Zel'dovich approximation; v_{th} turned out to be a factor of approximately 6 lower than the corresponding gravitational rms velocity dispersion. For comparison, the same simulation was run but without this thermal velocity component (models WDM t and WDM respectively in Table 1). The box size in both simulations was $7.5 h^{-1} \text{Mpc}$. The host halo chosen to be re-simulated within the multiple-mass scheme had a virial mass of $2 \cdot 10^{12} h^{-1} M_\odot$. The density profile of this halo is indistinguishable in both simulations. Regarding the guest halos, there is not any obvious difference between the halos from one simulation and the halos from the other one, although their density profiles are noisy and show a large scatter. Unfortunately, most of the guest halos have masses smaller than a few $10^9 h^{-1} M_\odot$ so that the number of particles in these halos is small (of the order of 10^3). In Figure 5 we plot the $c_{1=5}$ parameter versus the halo mass for halos from both simulations at $z = 0$. The introduction of a thermal velocity component had not any major effect on the inner density profiles and concentrations of halos within our resolution limits, even with a v_{th} two times larger than the corresponding

v_{th} for a warm non-relativistic mass $m_W = 605 \text{ eV}$. Nevertheless, we expect that for a large-enough particle velocity dispersion a shallow core will form in those halos that suffer a monolithic collapse. In the next section we study this case.

5. Thermal monolithic collapse and soft cores

There are two relevant conditions for the problem of halo formation, the initial fluctuation density profile which determines the kind of collapse the halo suffers and the amplitude of the velocity dispersion for the collapsing particles. The CDM halos form hierarchically and the particle tangential velocity dispersion is acquired since early epochs due to interactions of substructures with the global tidal field. In a WDM scenario, the first structures to collapse are those with masses close to M_f ; they assemble the mass M_f almost synchronously in a short time period (monolithic collapse). It is possible that structures formed by fragmentation also suffer monolithic collapse. As the collapse of halos less massive than M_f is delayed and the amount of substructure is small (compared to halos formed hierarchically), one expects a small tangential velocity dispersion in this case. On the other hand, WDM particles however have a residual thermal velocity dispersion. According to our results in x4.1 (see also Moore et al. 1999b), the density profiles of halos formed by monolithic collapse with a small amount of velocity dispersion (thermal) do not differ significantly from those produced hierarchically. In what case a significant soft core may form in the halos? Kinetic (thermal) energy plays a relevant role on the production of a soft core in the monolithic collapse, the core radius being larger as the energy content increases. Two ingredients allow to obtain a virialized soft core: 1) a monolithic collapse (top-hat density profile), and 2) a high particle 3-D velocity dispersion. We will prove that if both conditions are satisfied simultaneously, then the virialized density profile shows a soft core. The following heuristic model is a route to understand the role these ingredients play together.

Let us study the monolithic collapse of a sphere of mass M , radius R_M , and uniform density ρ_M at maximum expansion. We can introduce some kinetic energy assuming that all particles move on elliptical orbits with a given eccentricity e . Under these conditions, each particle orbits with the same period and any shell crossing is avoided. For purely radial motion, ($e = 1$), the collapse reaches a singular point. For $e < 1$, at maximum concentration, i.e. where each particle is found at periapsis, the collapse leads to a uniform sphere with radius $r^0 = R_M (1 - e) = (1 + e)$. The existence of this maximum concentration state is on the base of the existence of a soft core in the virialized halo. The tangential velocity at apapsis is:

$$v_t^2 = \frac{r^2 4 G_M (1 - e)}{3}; \tag{5}$$

while, at the maximum expansion, the kinetic energy T and the potential energy W are given by:

$$T = \frac{8}{15} \frac{G_M^2}{M} (1 - e) R_M^5 \tag{6}$$

$$W = \frac{16}{15} \frac{^2G}{M} R_M^5 ; \tag{7}$$

where the relationship between e, T and W is: $2T=W = 1 - e$.

The simplest approximation to estimate the virialized density at a given radius (density profile) is to assume a time average density at the same radius. This approach is based on the statistical hypothesis that the time average density is representative of the virialized halo density. Using the conventional parametric equations:

$$r = \frac{R_M}{(1+e)} (1 - e \cos \theta) \quad t = \frac{2\pi a^3}{4 G M (1+e)^3} (e \sin \theta); \tag{8}$$

the time average density at a radius r between r^0 and R_M is:

$$\langle \rho(r) \rangle = \frac{\int_0^R \rho(r;t) dt}{\int_0^R dt} = \frac{M (1+e)^3}{4 G M (1+e)^3} \int_0^R \frac{1}{(1 - e \cos \theta)^2} d\theta = \tag{9}$$

$$= \frac{M (1+e)^3}{(1 - e^2)^2} \left[\frac{2}{1 - e^2} - \frac{2}{1 - e^2} \operatorname{tg}^{-1} \left(\frac{1+e}{1 - e^2} \frac{e}{e + \dots} \right) \right]; \tag{10}$$

while between 0 and r^0 the average density is:

$$= M \left(\frac{1+e}{1 - e} \right)^{3=2} \tag{11}$$

where $\theta = 1 - (1+e)r=r_0$ and $\cos \theta = -e$. The constant density between 0 and r^0 is product of the particle (them all) angular momentum which prevents the particles from reaching the center. The constant density core mass is given by:

$$\frac{M_c}{M} = \left(\frac{1+e}{1 - e} \right)^{3=2} \tag{12}$$

A simple test of the statistical hypothesis on which our analytical model is based derives from N-body simulations. For example, in the limit of $T = 0$, eq. (10) shows that the profile shape in the inner part is $\propto r^{-1.5}$, only slightly steeper than that we have found in x4 (see also Moore et al. 1999b). With the aim to further explore the validity of the analytical solution, we have followed the non-linear evolution of a top-hat sphere with mass of $3.2 \cdot 10^{11} M_\odot$ and radius 50 kpc making use of the N-body technique. When the sphere reaches the maximum expansion, we inject uniform kinetic energy to the sphere, in order to obtain for $2T=W$ the values of 0.2 and 0.5. Figure 6 shows that there is a good agreement between the analytical solution for the density profile (solid lines) and the profile obtained with the N-body technique (empty circles). The upper (lower) curves are for $2T=W = 0.2$ (0.5). It is interesting to stress the relationship between T and the core size: the higher is T, the larger is the core radius.

We stress that soft cores in virialized dark collisionless halos may result only from two simultaneous conditions: (1) an initial shallow profile for the progenitor of the present structures

(monolithic collapse); (2) the presence of velocity dispersion. The angular momentum of kinetic motion avoids the migration of particles toward the center, limiting the central density.

We can use this simple model to give an estimate of the core mass in halos which suffer a hot monolithic collapse. We will think on the velocity dispersion as thermal velocity of the particles. The maximum expansion radius of a uniform sphere in a flat with cosmological constant universe is:

$$R_M = \left[\frac{32GM}{H_0^2 \rho_m 9^2} \right]^{1/3} \frac{1}{1+z_M}; \quad (13)$$

where ρ_m and H_0 are the matter density and the Hubble constant at $z = 0$, and z_M is the redshift at maximum expansion. At this epoch, thermal velocity is related to the $2T=W$ ratio by:

$$v_{th}^2 = \frac{3GM}{5R_M} \frac{2T}{W} \quad (14)$$

From eqs. (12), (13) and (14) we can derive the core mass:

$$M_c = \frac{10^9 - 5}{9} \left(\frac{5}{3} \right) \left[1 + \left(\frac{M_c}{M} \right)^{2=3} \right]^{3=2} \frac{v_{th}^3}{\rho_m H_0 G (1+z_M)^{3=2}} = \quad (15)$$

$$= 10^6 M_h^{-1} \left[1 + \left(\frac{M_c}{M} \right)^{2=3} \right]^{3=2} \frac{(v_{th}=km\ s^{-1})^3}{\rho_m (1+z_M)^{3=2}}; \quad (16)$$

where the term within square brackets contributes with a factor between 1 and 3.

For a warm ion of 0.6 keV, the filtering mass is $M_f = 10^{11} h^{-1} M_\odot$. For the cosmology used in this paper, the spherical top-hat model gives a collapse redshift of $z_c = 4.2 (1.5)$ for a $2 (1)$ fluctuation of $10^{11} h^{-1} M_\odot$ (see also x6.2), while the maximum expansion redshift is $z_m = 5.4 (3.0)$. At this redshift the thermal velocity is $v_{th} = 0.54 \text{ km/s} (0.34 \text{ km/s})$ (e.g., Narayanan et al. 2000). Therefore, from eq. (16) we obtain that the core mass for this fluctuation will be $M_c = 2.1 \cdot 10^4 h^{-1} M_\odot (1.1 \cdot 10^4 h^{-1} M_\odot)$, several orders of magnitude smaller than the core masses inferred from some observations. The thermal velocity of warm ions should be almost two order of magnitude larger in order to obtain soft cores comparable to observations. Therefore, only a very hot monolithic collapse of collisionless particles is able to produce soft halo cores.

6. Discussion

6.1. The formation of low-mass halos in simulations with a damped power spectrum

When the power spectrum of fluctuations is filtered above some wavenumber k_f , "pancakes" of size k_f^{-1} are the first structures to collapse and smaller objects are expected to form later by fragmentation (e.g., Zel'dovich 1970; Doroshkevich et al. 1980). The coupling between different modes in the non-linear gravitational evolution drives a transfer of power with power flowing from larger to smaller scales. This transfer is very efficient; numerical simulations confirmed such a behavior (e.g., Little, Weinberg, & Park 1991; Bagla & Padmanabhan 1997; White & Croft 2000).

Although our numerical experiments were not aimed at studying in detail the structure formation process, we noticed that indeed the first structures to collapse are those with scales close to the filtering scale R_f . These structures form smooth coherent filaments when they enter the non-linear regime (see also M elott & Shandarin 1990; Little et al. 1991, and more references therein) instead of the chains of dense clumps seen in CDM simulations. In the top-panel of Fig. 1 one may appreciate the filamentary structure of the protohalo that at $z = 1$ is just becoming non-linear. This structure collapses coherently roughly at the same time (monolithic collapse) but obviously the initial conditions are not spherically symmetric. However, matter flows towards the center of the filament and there some spherical symmetry is established (see the virialized halo at $z = 0$). Within the shrinking filament, substructure forms by fragmentation.

Based only on a visual inspection, we may say that the collapse of such substructure is almost parallel to the collapse of the filament. As mentioned above, the power transfer from larger to smaller scales is very efficient. It also seems that the collapse epoch of the fragmented halos is independent of their masses. Nevertheless, all these halos collapse on average later than in a CDM simulation. This might explain why the small WDM halos are less concentrated and why their concentrations, though with a large scatter, do not depend on mass (see Fig. 4). Because halos are less concentrated than in the CDM simulations, they are more easily disrupted. As it was shown in Paper I, the reduction of the number of small halos due to this effect is comparable to the effect that the power spectrum suppression has on this number, and both work together to deliver a very small number of satellites at $z = 0$.

Interestingly, our results suggest that on average and in a first approximation, the density profiles of dark matter halos are indeed universal, no matter how they form, either by hierarchical clustering or by a monolithic collapse or by fragmentation. The difference seen in their concentrations can be explained just as an effect of the formation epoch which for small WDM halos is delayed compared to the formation epoch of the corresponding CDM halos. As we have showed in x5, a way to affect significantly the inner density profile of halos in the case of a monolithic collapse is by including a high thermal velocity dispersion. The thermal velocities of warm ons of masses 1 keV are much smaller than this velocity dispersion.

6.2. Viability of the WDM scenario: observational tests

Because of the increasing evidence that the predictions of the nowadays standard CDM model at small scales are in conflict with observations, modifications to this scenario, able to retain their successful predictions at large scales, have been recently analyzed. As the nature of dark matter particles is still a mystery, it is tempting exchange CDM particles by WDM particles as the most simple modification to the standard scenario. At least from the point of view of the particle physics there is not an obvious preference for any of these particles (e.g., Colombi, Dodelson, & Widrow 1996). But, what are the advantages of the WDM scenario with respect to the CDM one from the point of view of structure formation?:

1. For a WDM model with $R_f > 0.1 \text{ Mpc}$ ($m_W < 1 \text{ KeV}$), $m = 0.3$, and $h = 0.7$, the observed circular velocity function of Milky Way and Andromeda satellites is roughly reproduced (Paper I).

2. Although in the WDM scenario the halos with masses close to or below M_f do not have a constant density core, they are less concentrated and have a density profile slightly shallower in the center (Paper I; x4 here). Recent observational studies have shown that with the current data is not possible to constrain with accuracy the halo inner density profiles of dwarf and low surface brightness (LSB) galaxies; these profiles are probably not steeper than r^{-1} and, if any, the concentrations of these halos are lower than those predicted in the CDM scenario (van den Bosch et al. 2000; Swaters, Moore & Trewheella 2000; van den Bosch & Swaters 2000). In Figure 7 we compare the $c_{1=5}$ concentration parameters of our guest WDM halos of model WDM t to the $c_{1=5}$ concentrations of dwarf and LSB galaxies, inferred from the observational data (see details in the figure caption). Unfortunately, there is not an overlap between the theoretical and observational data; nonetheless, it can already be appreciated that the guest WDM halos are in better agreement with observations.

3. The formation of disks within WDM halos ($m_W < 1 \text{ keV}$) in N-body+Hydrodynamic simulations does not seem to suffer from the disk angular momentum problem (Sommer-Larsen & Dolgov 2000).

On the other hand, listed below is a set of potential problems the WDM scenario faces successfully, giving probably even a better agreement with observations than CDM :

1. Several authors have shown that the Tully-Fisher (TF) relation of normal disk galaxies in the infrared band is an imprint of the mass-velocity ($M_h - V_{max}$) relation of CDM halos (Avila-Reese & Firmani 2000; Firmani & Avila-Reese 2000 and more references therein). For masses larger than $10 M_f$ there are not major differences between the CDM and the WDM halos (Paper I; see also Avila-Reese et al. 1998). How does the $M_h - V_{max}$ relation look for small masses? In Figure 8 we have plotted M_h versus V_{max} for our WDM models with $R_f = 0.2 \text{ Mpc}$. We also show in this figure the $M_h - V_{max}$ relation of guest halos obtained for a CDM simulation, its scatter and a linear fit to this relation (Avila-Reese et al. 1999). As expected, the WDM halos move towards the lower V_{max} side, but not dramatically and with a large scatter. The formation of dwarf galaxies may be strongly affected by feedback and reionization; these galaxies could lose some of their initial baryon matter through galactic winds (e.g., Mac Low & Ferrara 1999) or through photo-evaporation (Shapiro & Raga 2000) and thus see their luminosities diminished. In the TF plot this means that for a given luminosity, V_{max} shifts to larger values. Observations show that dwarf and normal galaxies have roughly the same infrared TF relation, if any, dwarf galaxies lie more on the low-velocity side and present more scatter (Pierini & Tully 1999; de Jong & Lacey 2000, quoted by Cole et al. 2000, see their Fig. 7). Therefore, the fact that for WDM the small halos are shifted in the $M_h - V_{max}$ relation as it is shown in Fig. 8 might resolve a potential problem of the CDM scenario. In conclusion, it seems that the WDM scenario can reproduce better the infrared

TF relation of dwarf galaxies than the CDM one.

2. Unlike in the CDM scenario, for WDM one expects that the satellite dwarf galaxies form later than the host large galaxies. The evolution of the substructure for our WDM simulation WDMt ($R_f = 0.2$ Mpc) is shown in Table 2. The scale factor normalized to one at present is given in the first column while the number of halos with maximum circular velocity V_{max} greater than 100 km/s is presented in column 2. Columns 4, 5, and 6 give the coordinates of the center of mass of the system composed by these halos. The total number of halos with $V_{max} > 15$ km/s that contain more than 200 particles and the mass of the most massive halo are given in columns 3 and 7, respectively. We see that the first structure starts to assemble at $z \approx 7$; this seed has a mass of $\approx 3 \times 10^{10} h^{-1} M_\odot$. The existence of collapsed structures at these epochs suggests that the reionization constraint should not be a problem for WDM models with $R_f > 0.1 - 0.2$ Mpc. Later, at $z \approx 4$, when the mass of the most massive halo has grown to $M_h \approx 1 \times 10^{11} h^{-1} M_\odot$, the first substructures appear by fragmentation. Thus, the building blocks for large galactic and supergalactic structures are those with masses near to M_f ; smaller structures (guest halos) form slightly later by fragmentation. We may say thus that the formation redshift of guest halos is approximately equal or less than $z_f(M_f)$. According to the linear theory and the spherical top-hat model, the typical formation redshift of halos of mass M will be $z_f(M) \approx z_0(M)^{1/3}$ for an Einstein-de Sitter cosmology; $z_0(M)$ is the variance calculated from the linear power spectrum and extrapolated to $z = 0$, and $\sigma_0 \approx 1.69$. For a flat cosmology with cosmological constant these formation redshifts are slightly larger. For example, using our CDM model with the power spectrum normalized to COBE, we have that $z_f(10^{11} h^{-1} M_\odot) \approx 1.5; 4.3; \text{ and } 7.0$ for 1, 2 and 3 peaks, respectively. If galaxies form from high peaks, then the typical formation redshifts of galaxies of $10^{11} h^{-1} M_\odot$ will be larger than $z = 2 - 3$ in our CDM cosmology. In the WDM models with $R_f < 0.2$ Mpc, smaller galaxies (dwarfs) will form around these redshifts.

From the observational point of view there are some pieces of evidence that dwarf galaxies formed earlier than bright galaxies. In the Local Group, all dwarf galaxies seem to have their oldest stellar population slightly younger than the oldest Milky Way halo population (Mateo 1998); for the Large Magellanic Cloud this age difference could be of 2 Gyr, according to studies of the horizontal branch morphology of stellar clusters (Olszewski, Suntzeff, & Mateo 1996, and references therein), while for the Small Magellanic Cloud the difference should be even larger since this galaxy seems to be younger than its neighborhood. On the other hand, comparisons of observed and modeled galaxy counts for Ly α dropout galaxies at $3.5 < z < 4.5$ suggest that some Ly α galaxies were already in place at $z \approx 4$ but dwarf galaxies may have formed later at $3 < z < 4$ (Metcalf et al. 2000), in agreement with predictions of the WDM scenario.

3. The Lyman forest is a powerful probe of the linear power spectrum on galactic and sub-galactic scales, upon the understanding that it traces the underlying matter density. Since in a WDM scenario the small-scales modes are damped out, one might think that the observed Lyman forest should not be reproduced by this cosmology. However, because of the efficient power transfer from larger to smaller scales (see x6.1), enough power on small scales is regenerated

at $z \approx 3-4$. Narayanan et al. (2000) have shown that WDM models ($m = 0.3$ and $h = 0.7$) with $R_f < 0.155$ Mpc ($m_w > 0.75$ keV) are able to reproduce the observed properties of the Lyman forest.

As we have seen, the WDM scenario works better than the CDM one in several aspects. Nonetheless, both scenarios fail in predicting soft halo cores and the independence of the halo central density on its mass, as some inferences from observations seem to suggest (e.g., Firmani et al. 2000a,b and the references therein). More observational data which explore in detail the inner structure of the halo component of galaxies are urgent, however, it is likely that the more solid data will come first from strong lensing studies of clusters of galaxies (the largest virialized structures). The only cluster for which a high-resolution mass map has been obtained shows a low central density value (Tyson, Kochanski, & Dell'Antonio 1998) similar to those inferred from dwarf and LSB galaxies (Firmani et al. 2000a,b). The phase space density of dark matter halos derived from observations also offers an important test for the WDM scenario (Hogan & Dalcanton 2000; Sellwood 2000). If more detailed observational studies confirm the existence of soft halo cores with the scaling properties suggested in Firmani et al. (2000a,b) and Sellwood (2000), the WDM scenario must be abandoned. Then alternatives such as the self-interacting CDM might result more appealing.

7. Summary and conclusions

We have carried out high-resolution N-body cosmological simulations for models with power spectrum damped at small scales and introducing a thermal velocity dispersion for the particles. We have also studied the "hot" monolithic collapse by means of an analytical model. Our main conclusions are:

- The density profiles of halos with masses near or below M_f are diverse although in average they are well described by the NFW profile. The only difference with the corresponding CDM halos is in their lower concentrations and probably in that their inner density profiles are not as steep as $r^{-1.5}$. Thus, though the cosmogony of the halos in both cases is rather different, the final virialized structures are not dramatically different.

- The concentrations of halos with masses near or below the filtering mass M_f are definitely smaller than those of the corresponding CDM halos. For halos more massive than a few times M_f , the concentrations and density profiles in the simulations with damped power spectrum and the CDM ones are similar. In the former case, the typical concentrations remain almost constant as the mass decreases below a few times M_f , while in the latter case concentrations monotonously increase with decreasing mass. The scatter of the concentration for a given mass is large in both cases. The difference in the concentrations of the small halos can be mainly explained by the relatively late formation epoch of small halos in the simulations with damped power spectrum at small scales.

- For our WDM models with filtering scales < 0.2 ($m_w > 0.6$ KeV), the thermal velocity

dispersions v_{th} are very small. Nevertheless, we explored whether its inclusion may have some influence on the halo structure. For a WDM model with $R_f = 0.2 \text{ Mpc}$ ($m_W = 605 \text{ eV}$) we used a v_{th} two times larger than the corresponding to this mass and we did not find any significant difference in the structure of the halos. Unfortunately, our resolution does not allow us to explore the small shallow core predicted analytically.

The inner structure of dark matter halos formed through monolithic collapse can be affected only if the particles have significant velocity dispersions. A simple analytical model for the spherical top-hat collapse with non-zero kinetic energy (tangential velocity) at maximum expansion shows that a shallow core forms in the virialized halo, and its size is directly related to the initial kinetic energy or periapsis-to-apapsis ratio of the orbits. We have further estimated the velocity dispersion necessary to produce shallow cores in the WDM halos supposed to collapse monolithically. The thermal velocity dispersion of warm ions should be almost 100 times larger in order to form shallow cores of the size inferred from some observations.

We conclude that a flat WDM model with $R_f = 0.16 \text{ Mpc}$ ($m_W = 750 \text{ eV}$), $\beta = 0.7$, and $h = 0.7$, has several advantages over the corresponding CDM model. The problem of excess of substructure is solved (Paper I), the halos of dwarf and LSB galaxies result less concentrated than in the CDM scenario as observations suggest (Fig. 7), and the disk angular momentum problem is alleviated (Sommer-Larsen & Dolgov 2000). Furthermore, our preferred WDM model describes better than CDM the Tully-Fisher relation of dwarf galaxies (Fig. 8) and the formation epochs of these galaxies (Table 2, x6). On the other hand, this model is not apparently in conflict with measurements of the power spectrum of Lyman forest (Narayanan et al. 2000) and with the reionization constraints (Bode et al. 2000). Nonetheless, the WDM model is ruled out if more observations confirm the existence of soft halo cores as well as the independence on mass of their densities; the crucial test is at cluster scales. No doubt, exciting questions remain to be answered in the near future.

We are grateful to Anatoly Klypin and Andrey Kravtsov for kindly providing us a copy of the ART code in its version of multiple mass. We also thanks Anatoly Klypin for enlightment discussions. E.D. thanks the Fondazione Cariplo for financial support. Our ART simulations were performed at the Direccion General de Servicios de Computo Academico, UNAM, using an Origin-2000 computer.

REFERENCES

- Aguilar, L., Merritt, D. 1990, *ApJ*, 354, 33
- Avila-Reese, V., & Fimani, C. 2000, *RevMexA&A*, 36, 23
- Avila-Reese, V., Fimani, C., & Hernandez, X. 1998, *ApJ*, 505, 37

- Avila-Reese, V., Fimani, C., Klypin, A., & Kravtsov, A.V. 1999, *MNRAS*, 310, 527
- Balbi, A. et al. 2000, preprint (astro-ph/0005124)
- Bagla, J.S., & Padmanabhan, T. 1997, *MNRAS*, 286, 1023
- Bardeen, J.M., Bond, J.R., Kaiser, N., & Szalay, A.S. 1986, *ApJ*, 304, 15
- Blumenthal, G.R., Pagels, H., & Primack, J.R. 1982, *Nature*, 299, 37
- Bode, P., Ostriker, J.P., & Turok, N. 2000, preprint (astro-ph/0010389)
- Burkert, A. 1995, *ApJ*, 477, L25
- Carlberg, R.G., Yee, H.K.C., Ellingson, E., Abraham, R., Gavel, P., Morris, S., Pritchet, C.J. 1996, *ApJ*, 462, 32
- Cole, S., Lacey, C.G., Baugh, C.M., & Frenk, S.F. 2000, preprint (astro-ph/0007281)
- Colín, P., Avila-Reese, V., & Valenzuela, O. 2000, *ApJ*, 542, 622 (Paper I)
- Columbi, S., Dodelson, S., & Widrow, L.M. 1996, *ApJ*, 458, 1
- de Bernardis, P. et al. 2000, *Nature*, 404, 955
- de Blok W.J.G., & McGaugh S.S., 1997, *MNRAS*, 290, 533
- Doroshkevich, A.G., Kotok, E.V., Novikov, I.D., Polyudov, A.N., Shandarin, S.F., & Sigov, Yu.S. 1980, *MNRAS*, 192, 321
- Eke, V.R., Cole, S., Frenk, C.S., & Henry, P.J. 1998, *MNRAS*, 298, 1145
- Fimani, C., & Avila-Reese, V. 2000, *MNRAS*, 315, 457
- Fimani, C., D'Onglia, E., Avila-Reese, V., Chincarini, G., & Hernandez, X. 2000a, *MNRAS*, 315, L29
- Fimani, C., D'Onglia, E., Chincarini, G., Hernandez, X., & Avila-Reese, V. 2000b, *MNRAS* in press (astro-ph/0005001)
- Flores, R., & Primack, J.R. 1994, *ApJ*, 427, L1
- Hannestad, S., & Scherrer, R.J. 2000, *Phys.Rev.D* 62, 043522
- Hogan, C.J. 1999, preprint (astro-ph/9912549)
- Hogan, C.J., & Dalcanton, J.J. 2000, *Phys.Rev.D* 62, 063511
- Kamionkowski, M., & Liddle, A.R. 1999, preprint (astro-ph/9911103)

- Kau mann , G ., W hite, S.D .M ., & Guideroni, B .1993, M N R A S , 264, 201
- K lypin, A A ., K ravtsov, A V ., Valenzuela, O ., P rada, F .1999, A p J , 522, 82
- K lypin, A A ., & H oltzman, J .1997, preprint (astro-ph/9712217)
- K lypin, A A ., K ravtsov, A V ., Bullock, J ., & P rim ack, J .2000, preprint (astro-ph/0006343)
- K ravtsov, A V ., K lypin, A A ., & K hokhlov, A M .1997, A p J S 111, 73
- L in, W B ., H uang, D H ., Z hang, X ., & B randenberger, R .2000, preprint (astro-ph/0009003)
- L ittle, B ., W einberg, D H ., & P ark, C h .1991, M N R A S , 253, 295
- M ac L ow , M .M ., & F errara, A .1999, A p J , 513, 142
- M ateo, M .L .1998, A R A & A , 36, 435
- M elott, A L ., & S handarin, S F .1990, N ature, 346, 633
- M etcalfe, N ., S hanks, T ., C ampos, A ., M cCracken, H J ., & F ong, R .2000, preprint (astro-ph/0010153)
- M oore, B .1994, N ature, 370, 629
- M oore, B ., G higna, S ., G overnato, F ., L ake, G ., Q uinn, T ., S tadel, J ., & T ozzi, P .1999a, A p J , 524, L19
- M oore, B ., Q uinn, T ., G overnato, F ., S tadel, J ., & L ake, G .1999b, M N R A S , 310, 1147
- N arayanan, V K ., S pergel, D N ., D ave, R ., & M a, C h-P .2000, preprint (astro-ph/0005095)
- N avarro, J F ., F renk, C S ., & W hite, S D M .1997, A p J , 490, 493
- O lszwesi, E W ., S untze , N B , & M ateo, M .1996, A R A & A , 34, 511
- P eacock, J ., & D odds, S .1994, M N R A S 267, 1020
- P erlm utter, S .et al.1999, A p J , 517, 565
- P ierini, D ., & T u s, R J .1999, a, 343, 751
- P ierpaoli, E ., B organi, S ., M asiero, A ., & Y am aguchi, M .1998, P hysR ev D , 57, 2089
- R iess, A G .et al.1998, A J , 116, 1009
- S hapiro, P R ., & R aga, A C .2000, in \A strophysical P lasm as: codes, m odels, and observations", eds. J .A rthur, N .B rickhouse, & J .Franco, R ev M ex A & A Serie de C onferencias, 9, 292
- S ellwood, J A .2000, A p J , 540, L1

Schmidt, B. P. et al. 1998, *ApJ*, 507, 46

Sommer-Larsen, J., & Dolgov, A. 2000, preprint (astro-ph/9912166)

Swaters, R. A., Madauro, B. F., & Trewhella, M. 2000, *ApJ* in press (astro-ph/0001277)

Tittley, E. R., & Couchman, H. M. P. 1999, preprint (astro-ph/9911365)

Tyson J. A., Kochanski G. P., & Dell'Antonio I. P. 1998, *ApJ*, 498, L107

van den Bosch, F. C., & Swaters, R. A. 2000, preprint (astro-ph/0006048)

van den Bosch, F., Robertson, B. E., Dalcanton, J. J., & de Blok, W. J. G. 1999, *AJ* submitted (astro-ph/9912004)

van Kampen, E. 2000, preprint (astro-ph/0008453)

White, M., & Croft, R. A. C. 2000, *ApJ*, 539, 437

Zeldovich, Y. B. 1970, *a*, 5, 84

Table 1. Models and Simulations Parameters

R_f (M pc)	Model	v_{th} (km/s)	m_p ($h^{-1}M_\odot$)	Box ($h^{-1}Mpc$)	Resolution ($h^{-1}kpc$)	N_{host}
0.2	WDM _t	6.7	2:1 10^6	7.5	0.1	1
0.2	WDM	0.0	2:1 10^6	7.5	0.1	1
1.7	WDM _{7.5}	0.0	2:1 10^6	7.5	0.4	1
1.7	WDM ₁₅	0.0	1:7 10^7	15.0	0.4	1
1.7	WDM ₃₀	0.0	1:3 10^8	30.0	1.8	4
1.7	WDM ₆₀	0.0	1:1 10^9	60.0	1.8	4
0.0	CDM ₆₀	0.0	1:1 10^9	60.0	1.8	4

Table 2. Substructure evolution in model WDM_t

Epoch	$N_{h>100}$	N_N	X_{cm} ($h^{-1}Mpc$)	Y_{cm} ($h^{-1}Mpc$)	Z_{cm} ($h^{-1}Mpc$)	M_h ($h^{-1}M_\odot$)
1.000	1	13	7.193	5.236	1.406	1:4 10^{12}
0.879	1	11	7.191	5.287	1.424	1:3 10^{12}
0.753	1	17	7.175	5.349	1.443	1:1 10^{12}
0.630	2	24	7.153	5.453	1.452	6:6 10^{11}
0.504	4	24	7.191	5.454	1.626	5:2 10^{11}
0.405	4	29	7.139	5.705	1.516	4:9 10^{11}
0.354	5	26	7.155	5.740	1.528	2:9 10^{11}
0.303	4	20	7.170	5.875	1.472	2:4 10^{11}
0.255	3	15	0.379	5.837	1.515	1:8 10^{11}
0.204	2	6	7.117	6.623	1.055	1:1 10^{11}
0.153	2	2	7.135	6.148	1.406	5:2 10^{10}
0.129	1	1	7.151	6.994	0.650	2:7 10^{10}

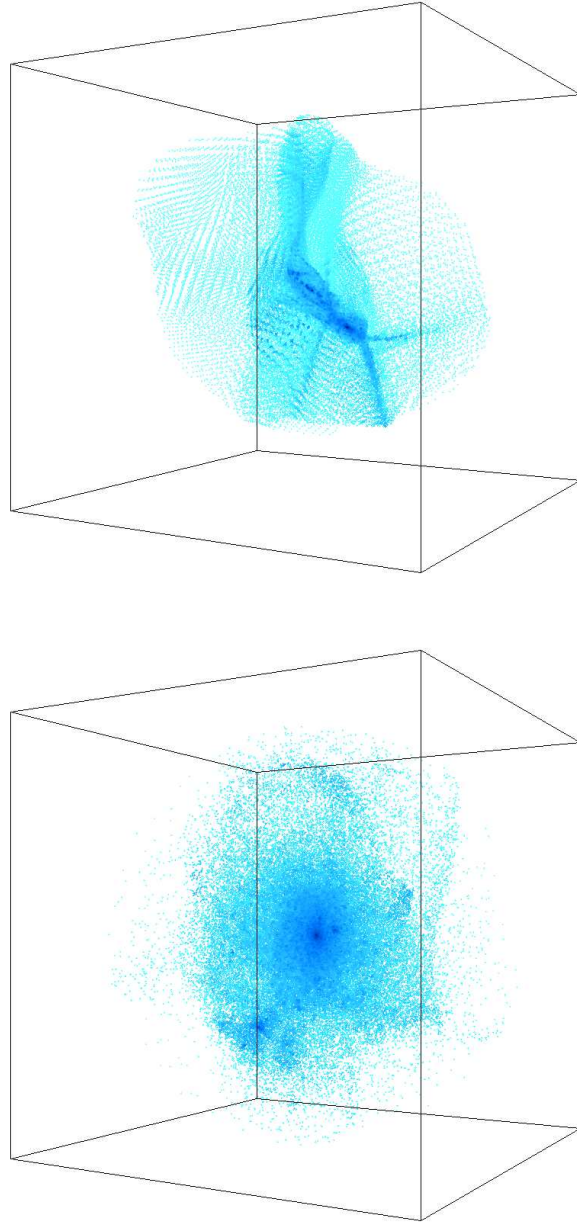


Fig. 1. The distribution of dark matter particles inside a sphere of radius $1.5 h^{-1} M_{\text{pc}}$ centered on a host halo from simulation WDM₆₀ at $z = 0$ is shown in the bottom panel. These particles are traced back to $z = 1$ and plotted there in the top panel. All of them lie within a sphere of radius $5.6 h^{-1} M_{\text{pc}}$ comoving centered on the center of mass of the particle system. The mass of this halo is about half the corresponding filtering mass ($M_f = 1.7 \cdot 10^{14} h^{-1} M_{\odot}$) and it was one of the first structures to collapse in the simulation. Note that the virialized halo emerges from the fragmentation of a filament that lies on a pancake.

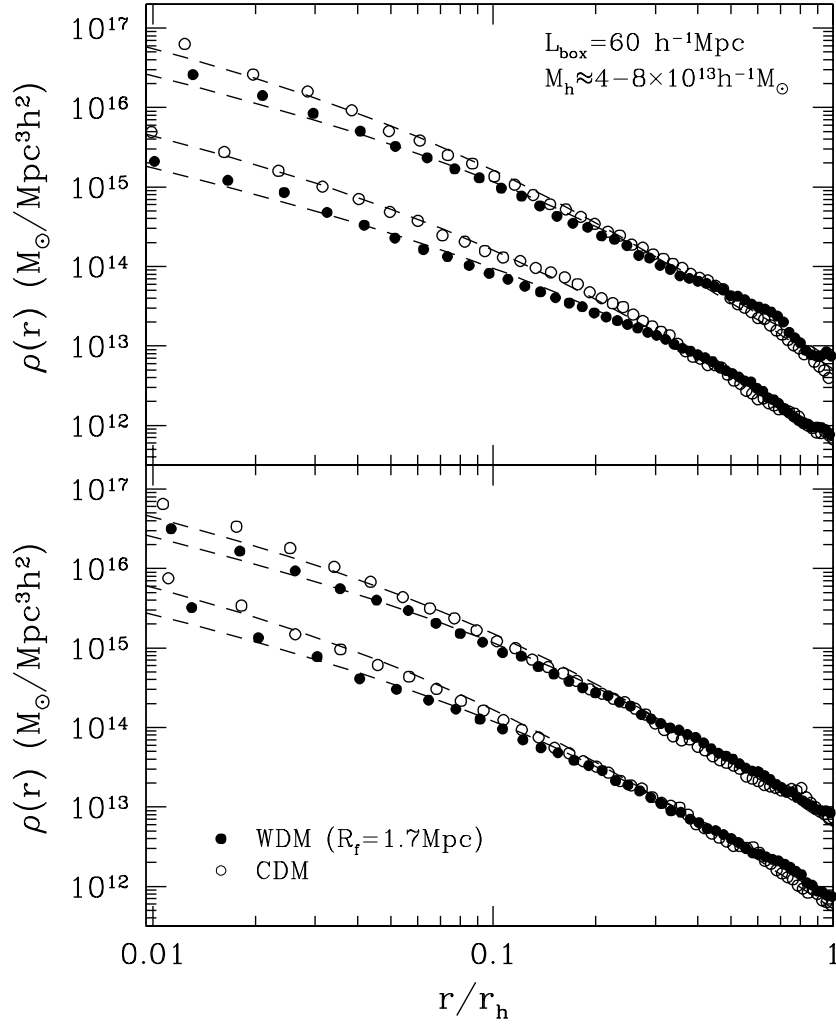


Fig. 2. | Density profiles of the four host halos in simulations WDM₆₀ (solid circles) and CDM₆₀ (empty circles). The dashed lines are NFW fits to these profiles. Radii are normalized to the corresponding halo (virial) radius. The inner point in each plotted density profile corresponds to four times the formal force resolution. The masses of the WDM halos are 2-4 times smaller than the filtering mass $M_f = 1.7 \cdot 10^{14} \text{ h}^{-1} \text{M}_\odot$.

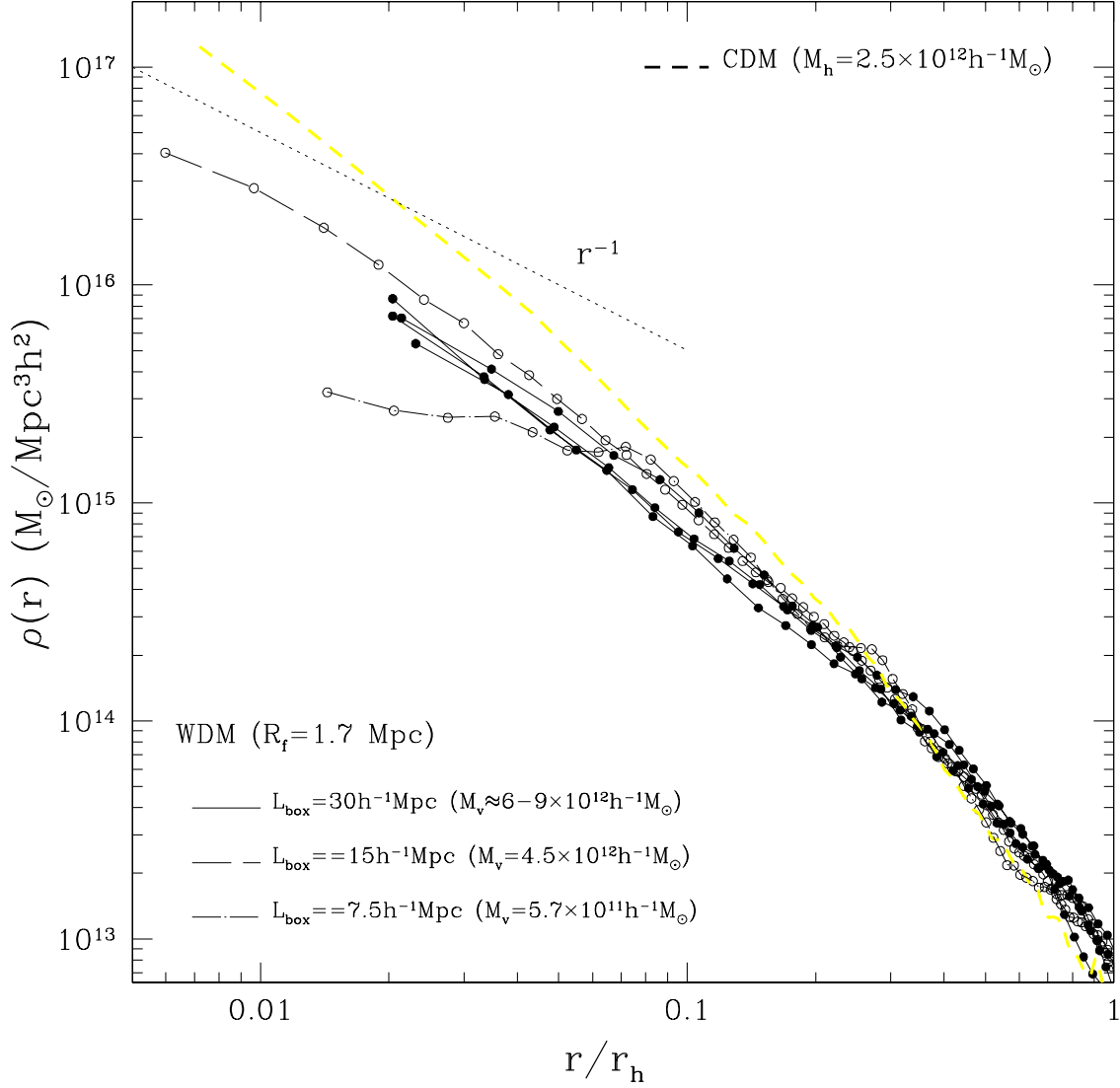


Fig. 3. | Density profiles of host halos in simulations WDM₃₀ (solid lines), WDM₁₅ (long-dashed line), WDM_{7.5} (dot-dashed line), and for a CDM halo reported in Paper I (thick short-dashed line). The inner points and the normalization of the radius are as in Fig. 2. The masses of the halos are shown in the panel. As one expects, the density profile of the halo in the WDM_{7.5} simulation resulted affected due to the small size of the box (see x3).

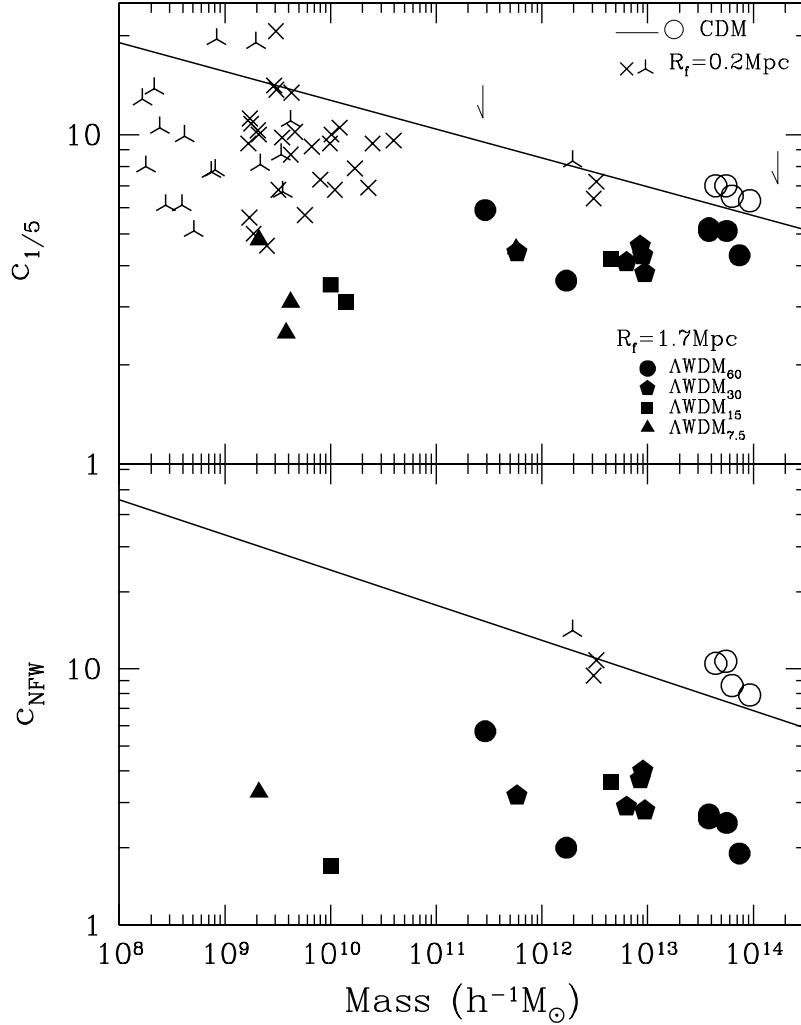


Fig. 4. | The $C_{1/5}$ and C_{NFW} concentration parameters vs. halo mass (upper and lower panels respectively) from the WDM simulations with $R_f = 1.7$ Mpc (solid symbols) and $R_f = 0.2$ Mpc (crosses and skeletal triangles, from Paper I and the model WDM presented here respectively), and from the CDM₆₀ simulation (empty circles). The solid line is a linear fit for thousands of isolated halos obtained in a CDM simulation (Avila-Reese et al. 1999). The vertical arrows indicate the "filtering" masses M_f corresponding to $R_f = 0.2$ and 1.7 Mpc. The C_{NFW} parameter for the guest halos in the simulations of Paper I and the model WDM presented here are not shown because the number of particles of these halos is too small and the dispersion in the NFW fit resulted too big. Note that the concentration parameters of halos below M_f remain almost constant as the mass decreases while in the case of the CDM model these concentrations continuously increase as the mass decreases.

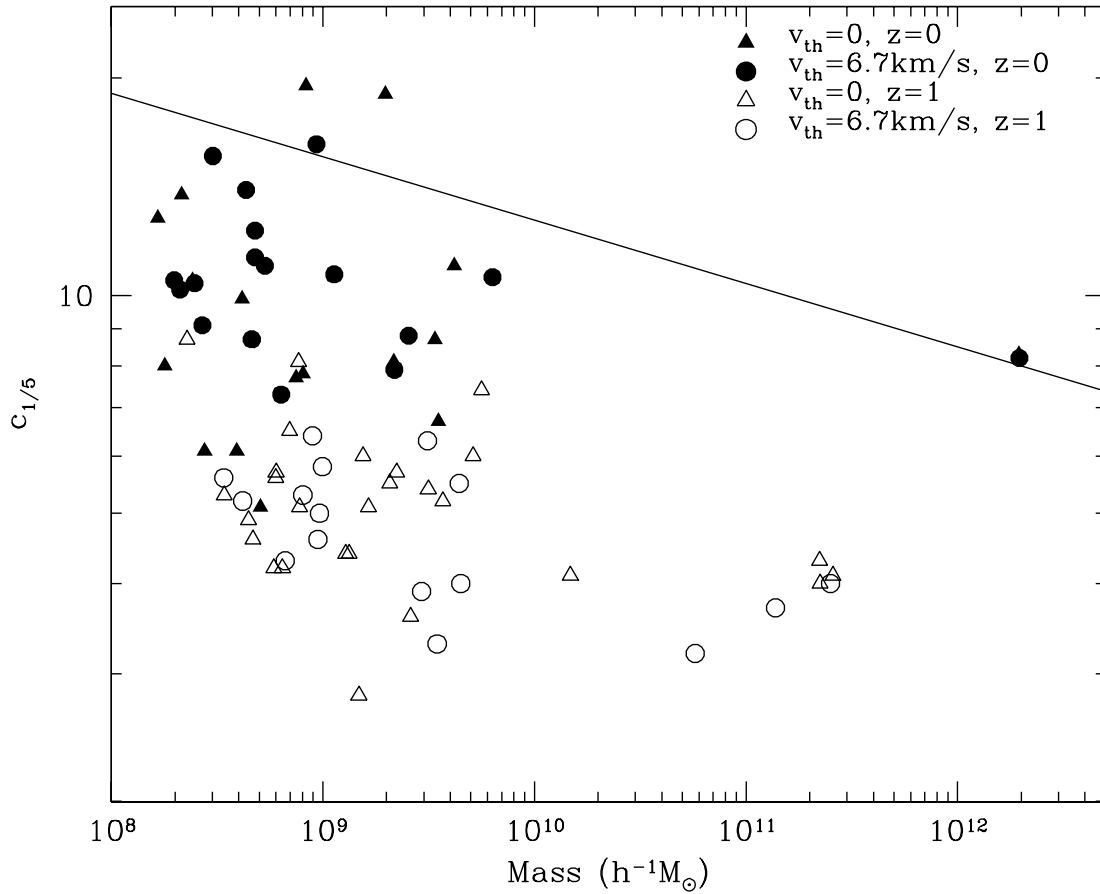


Fig. 5. | The $c_{1/5}$ concentration parameter vs. halo mass from WDM simulations ($R_f = 0.2$ Mpc, $L_{\text{box}} = 7.5 h^{-1} \text{Mpc}$) with $v_{th} = 0$ (run WDM triangles) and with $v_{th} = 6.7 \text{ km/s}$ (determined at $z_i = 40$ (run WDM circles)); this velocity is two times larger than that corresponding to the m_W associated to the used R_f . The filled symbols are for halos at $z = 0$ while the empty symbols are for halos at $z = 1$. There is not any significant difference in between simulations with and without thermal velocity inclusion.

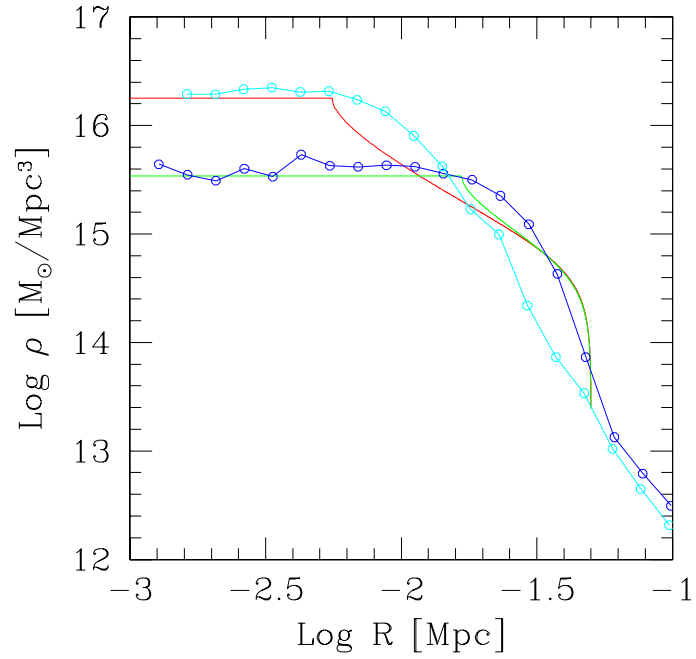


Fig. 6. Comparison of the density profile derived from an analytical model (eq. 9) (solid lines) with that obtained in a N-body simulation for a top-hat sphere of $3.2 \cdot 10^{11} M_{\odot}$ and radius 50 kpc, adding uniform thermal energy at the maximum expansion (empty circles). For both approaches, N-body and analytical model, the ratio $2T=W$ is 0.2 (upper curves) and 0.5 (lower curves).

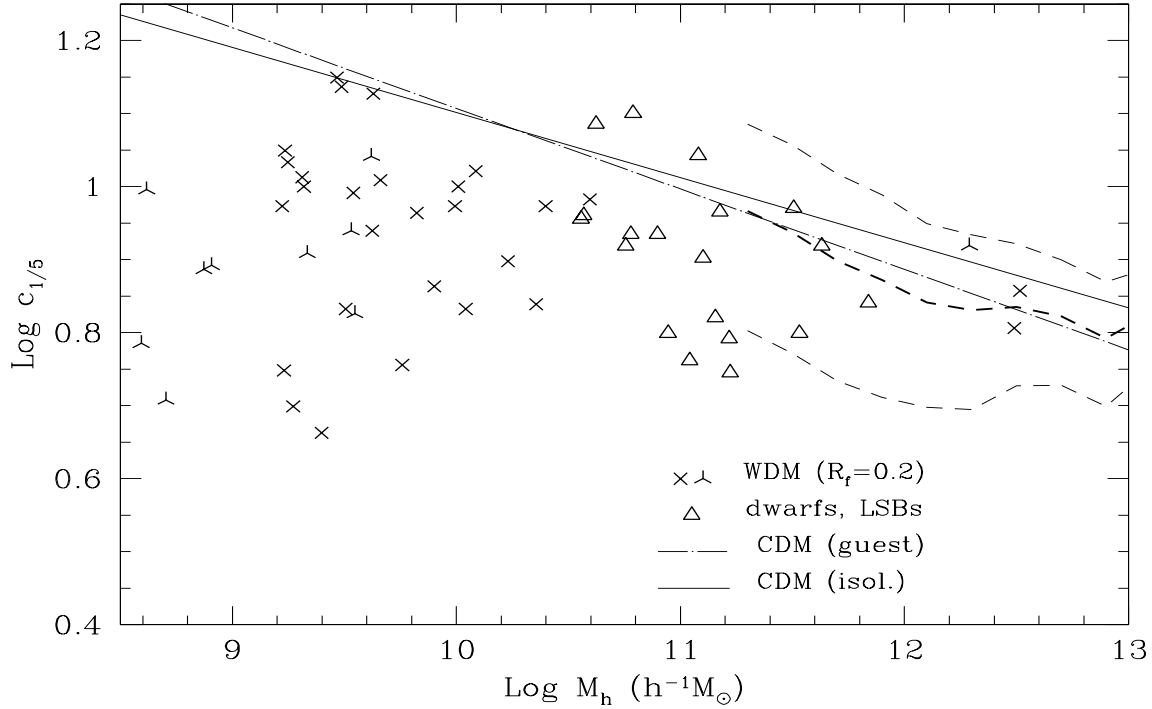


Fig. 7. | A comparison of the $c_{1=5}$ concentration parameters of WDM halos ($R_f=0.2$ M pc, crosses and skeletal triangles) with those inferred from the rotation curves of dwarf and LSB galaxies (triangles). Crosses correspond to a run presented in Paper I ($L_{\text{box}} = 15h^{-1}\text{M pc}$, while skeletal triangles are from the run WDM presented here ($L_{\text{box}} = 7.5h^{-1}\text{M pc}$). The dashed lines are the average concentrations and standard deviations of guest halos found in a CDM simulation (Avila-Reese et al. 1999). The dot-dashed line is a linear fit to these data, while solid line is the linear fit to data corresponding to isolated halos in the same simulation. The observational data for dwarf galaxies were taken from van den Bosch & Swaters 2000 who fit the halo component of their rotation curve decompositions to a NFW profile finding this way ρ_{FW} . We pass from c_{NFW} to $c_{1=5}$ and take into account the difference in the definition of virial radius of van den Bosch & Swaters with our definition (the difference in $c_{1=5}$ is not more than a factor of 1.05 larger with our definition respecting that of these authors). The mass of the halos is calculated from the V_{200} reported by them: $M_h [h^{-1} M_{\odot}] = 4.2 \cdot 10^5 V_{200}^3 [\text{km/s}]$. We have used only those galaxies for which a meaningful fit to the NFW is found. For the LSB galaxies, data from van den Bosch et al. 2000 were used. The same procedure described for the dwarf galaxies was used. We have considered only those galaxies for which the estimated V_{200} is smaller than the measured V_{max} . Unfortunately, WDM models and observations do not significantly overlap. Nevertheless, one already sees that the halos of dwarf and LSB galaxies are in average less concentrated than the CDM ones, being in better agreement with the WDM halos.

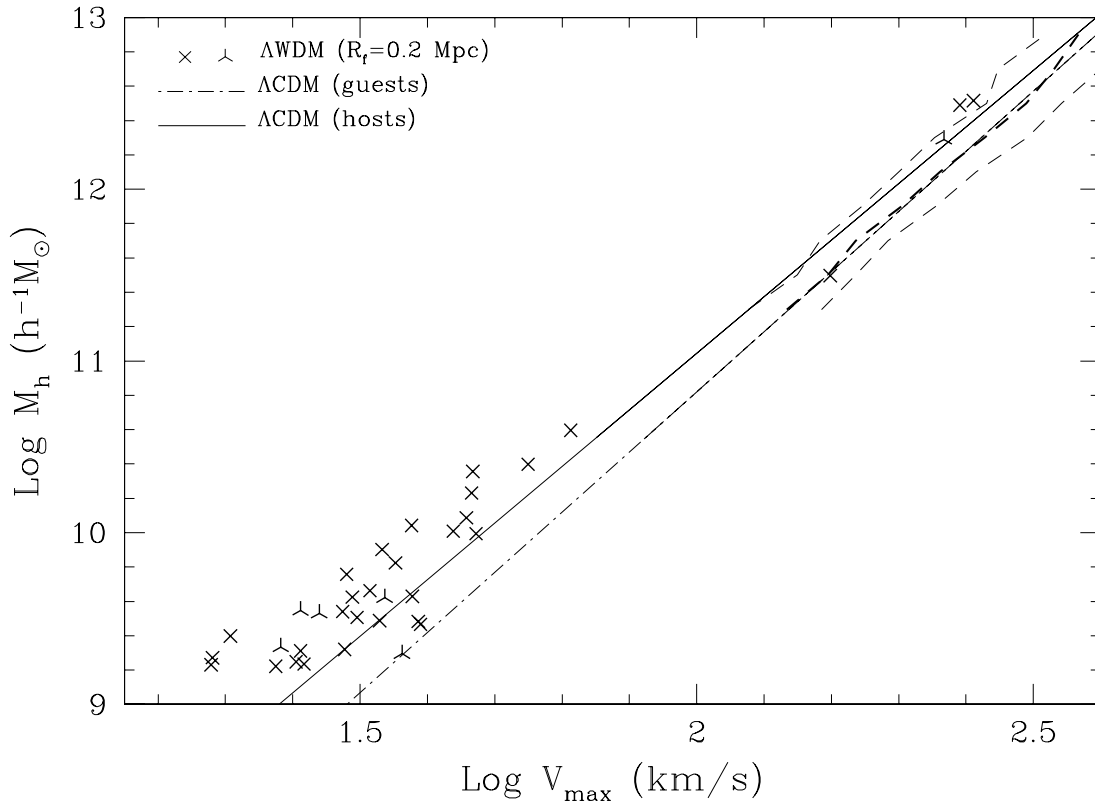


Fig. 8. | The halo mass vs. its maximum circular velocity for the the same runs presented in Fig. 4 and 6 (Λ WDM model with $R_f = 0.2$ Mpc; crosses and skeletal triangles). For comparison, we also plot the mass-velocity relation and its dispersion for guest halos (dashed lines) found in a Λ CDM simulation, a linear fit to this relation (dot-dashed line), and a linear fit corresponding to isolated halos (solid line) (see Avila-Reese et al. 1999).